Preliminary test results of LAr prototype detector *

Pei-Xian Li(李佩弦)[1,2;1)] Meng-Yun Guan(关梦云)[1] Chang-Gen Yang(杨长根)[1] Peng Zhang(张鹏)[1]
Jin-Chang Liu(刘金昌)[1] Yong-Peng Zhang(张永鹏)[1,2] Cong Guo(郭聪)[1,2] Yi Wang(王毅)[1,2]

[1]Institute of High Energy Physics, Chinese Academy of Sciences, Beijing 100049, China
[2]University of Chinese Academy of Sciences, Beijing 100049, China

Abstract: Liquid argon (LAr) is an attractive target for the direct detection of WIMPs. A LAr prototype detector was designed to study the technology and properties of LAr detectors. The prototype detector had an active volume containing 0.65 kg of liquid argon. A liquid nitrogen (LN) cooling system allowed the temperature fluctuation of the liquid argon to be controlled within less than 0.1 K during a one month run. In the ^{22}Na calibration run, the LAr prototype obtained 1.59±0.02 p.e./keV light yield for 511 keV gamma rays using a domestic-made argon purification system.

Keywords: LAr technology, LAr purification, light yield, dark matter

PACS: 95.35.+d, 29.40.-n **DOI:** 10.1088/1674-1137/40/11/116005

1 Introduction

The data from Planck [1] provided compelling evidence for a significant cold dark matter component in the composition of the Universe. Weakly interacting massive particles (WIMPs) are a well-motivated galactic dark matter candidate. Numerous direct detection experiments [2–9] have been or are being developed to detect WIMPs. Liquid argon (LAr) detectors are attractive detectors for the direct detection of WIMPs [7, 8, 10].

Liquid argon is an excellent scintillation material, with a high light yield of approximately 40 photons per keV [11]. Liquid argon provides outstanding pulse-shape discrimination (PSD) based on scintillation timing. The excitation and ionization of the medium from particles interacting with argon atoms leads to two excited states, with 6 ns for the singlet state and 1.6 μs for the triplet state [12] respectively. With sufficient photon statistics, PSD allows discrimination of nuclear recoil events from electron-induced background events at better than 10^8 [5, 13–15], which provides a way to detect rare nuclear recoil events.

The LAr detector is not only an attractive detector for the direct detection of WIMPs, but is also widely used for other research. A LAr detector was used as the calorimeter in the ATLAS experiment [16], and recently a LAr detector was proposed to be the veto detector of the CDEX-10 experiment [9]. The work presented in this paper aimed at setting up a LAr detector prototype, especially studying the technology of liquification and purification, which will be necessary for ton-scale liquid argon detectors in the future.

2 LAr prototype detector design and structure

The liquid argon prototype detector, shown in Fig. 1, consisted of a double wall vacuum stainless steel cryostat and a polytetrafluoroethylene (PTFE) vessel which contained 0.65 kg active liquid argon. This PTFE vessel was completely immersed in a liquid argon bath contained in a inner LAr container located in the cryostat. The PTFE vessel consisted of a PTFE cylinder and two fused silica windows. The cylinder was 9.2 cm high, with 8.0 cm inner diameter, and 1.0 cm wall thickness. The PMTs were immersed in the outer LAr bath.

The central wavelength of the argon scintillation light was 128 nm, so 1,1,4,4-tetraphenyl-1,3-butadiene (TPB) was needed as a wavelength shifter to convert the 128 nm scintillation photons to the wavelength for detection by photomultipliers. The peak of the TPB emission wavelength is 420 nm [17]. About 200 μg/cm^2 [7] TPB was deposited onto the inner surface of the PTFE cylinder and the inner surfaces of the fused silica windows in a thermal vacuum coating device.

The wavelength-shifted light was detected by two PMTs, shown in Fig. 1. A Hamamatsu R8520-06 mod

Received 5 February 2016, Revised 10 May 2016

∗ Supported by China Ministry of Science and Technology (2010CB833003), National Nature Science Foundation of China, Youth Science Found (11305188)

1) E-mail: lipeixan@ihep.ac.cn

PMT (1") was installed in the top, and a Hamamatsu R11065 PMT (3") installed in the bottom. About 1 mm layer of LAr optically coupled the PMTs to the fused silica windows. The room-temperature quantum efficiency of the R11065 was 25% at 420 nm [18]. It was run at a typical gain of 4.2×10^6. The signal of the 1" PMT was only used as the coincidence with the 3" PMT to generate the trigger. The signals of the 3" Hamamatsu R11065 PMT were recorded for analysis. The PMT effective coverage (Hamamatsu report effective area [18]) of our detector was about 9.6%.

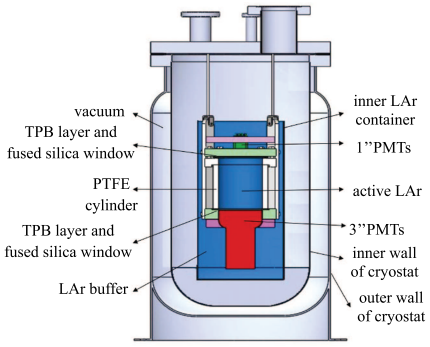

Fig. 1. (color online) Structure of liquid argon prototype detector. The outer layer was a double wall vacuum stainless steel cryostat. The PTFE vessel was immersed in a liquid argon bath. The red and green parts show the 3" PMT and 1" PMTs. The blue parts show the liquid argon.

3 Cooling, purification and recirculation system

The liquid nitrogen (LN) cooling system, shown in Fig. 3, consisted of a 100 L liquid nitrogen dewar and a cold-head. Since the boiling point of liquid nitrogen is about 10 K lower than that of liquid argon at the same pressure, the liquid nitrogen could be used to liquefy the gaseous argon. The cold-head was inside the cryostat. The 100 L liquid nitrogen dewar was connected to the cold-head through a lengthy bellow. The liquid nitrogen went into the cold-head and removed the latent heat to give cooling capacity. The cooling power could be adjusted though controlling the vaporized nitrogen flow. Using the pressure of the LAr cryostat as the process variable, a commercial proportional-integral-derivative (PID) controller was used to control the temperature of the LAr. Test results showed the LAr temperature fluctuation was less than 0.1 K in a one month run.

To obtain the maximum light yield,the dissolved electronegative impurities such as nitrogen, oxygen, and water vapour needed to be lower than 0.1 ppm [19]. A special domestic-made purification system, which was developed by Beijing Beiyang United Gas Co., Ltd , combined with a gas recirculation loop, could fulfill the demand. Before filling the argon, the LAr cryostat was evacuated for several days, with the pressure of the cryostat maintained at about 10^{-4} Pa. Then the feed argon gas (99.9995%) was purified by the purification system and flowed to the LAr container, shown in Fig. 3. After filling with liquid argon, the argon was recirculated to further improve the argon purity. The liquid argon was vaporized by a heater installed at the bottom of the inner LAr container. An advanced aerospace metal bellows pump was used to drive the argon gas to recirculate through the purification system to flow back to the cold-head to be liquefied again. Argon gas passed through the purification system several times until the scintillation light yield was not improved further.

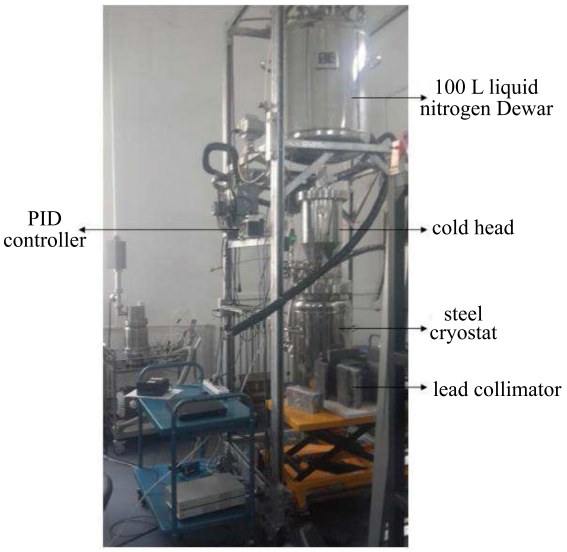

Fig. 2. The LN cooling system together with the prototype detector system.

Fig. 3. Purification system, developed by Beijing Beiyang United Gas Co., Ltd, designed for reducing nitrogen, oxygen, and water impurities to lower than 0.1 ppm levels.

4 DAQ system and single-photoelectron calibration

A LeCroy Waverunner 610Zi oscilloscope [20] was used to record the signals waveform from the 3" PMT for off-line analysis. The trigger required a coincidence of the 1" PMT and the 3" PMT signals within 300 ns. The threshold of the 3" PMT was 10 mV in the source calibration run (5 mV in single-photoelectron calibration run), and that of the 1" PMT was 6 mV in the source calibration run. When an event satisfied the trigger condition, only the signals of the 3" PMT in a 10 μs time window (1.6 μs before the trigger, 8.4 μs after the trigger gate), were stored on a local hard disk.

To measure the light yield of the LAr prototype detector, the single-photoelectron spectrum was used to calibrate the gain of the Hamamatsu R11065 PMT. A LED installed in the detector was driven by a BNC 8010 pulse generator. The width of the gate for the single-photoelectron calibration run was 200 ns. The trigger was generated by the BNC 8010 synchronized with the LED. A typical single-photoelectron charge spectrum of the Hamamatsu R11065 PMT is shown in Fig. 4.

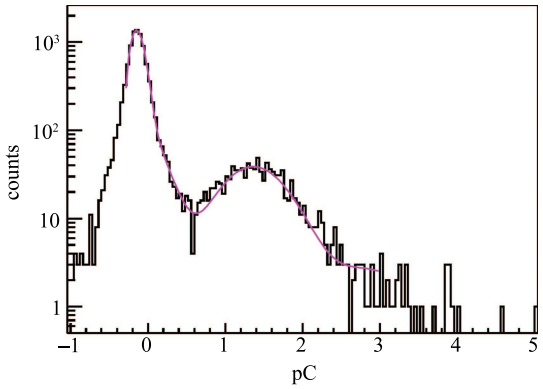

Fig. 4. The single-photoelectron spectrum of the Hamamatsu R11065 PMT was obtained by the LED calibration in the LAr prototype detector. The spectrum was fitted with Eq. (2). About 1.43±0.02 pC/PE was obtained.

The number of photoelectrons (p.e.) induced by each incident light pulse follows a Poisson distribution and the probability of having n photoelectrons is expressed as:

$$P(n) = \mu^n \cdot \frac{\mathrm{e}^{-\mu}}{n!}, \tag{1}$$

where the mean value μ is determined by the light intensity. To make sure the most of the signals were from a single photoelectron, the LED light was adjusted to a proper intensity. Experimentally, the PMT response to photoelectrons could be roughly treated as a series of Gaussian functions of different weights. In this measurement ,a simplified fit function $f(x)$ was used [21]:

$$f(q) = c_0 \times G(q, \mu_0, \sigma_0) + c_1 \times G(q, \mu_0 + \mu_1, \sqrt{\sigma_0^2 + \sigma_1^2}) \tag{2}$$

where $\mathrm{G}(x,\mu,\sigma)=\mathrm{e}^{\frac{-(x-\mu)^2}{2\sigma^2}}$ is a standard Gaussian function. The first term describes the pedestal with a mean value and width of μ_0 and σ_0, respectively. Similarly the second term represents the single photoelectrons peak, with its mean value and width properly related. In Fig. 4, about 1.43±0.02 pC/PE was obtained.

5 Event analysis and light yield

The signal baseline was determined and subtracted from the signal waveform of the Hamamatsu R11065 PMT. The average of the digitized samples in the 1.6μs pro-trigger (where no signal was expected) was calculated. Once the baseline has been subtracted, the integral was evaluated for the waveform to give the charge of the event.

The detector was exposed to a 70 μCi ^{22}Na gamma source. The main gamma energies of the ^{22}Na source were 511 keV and 1274 keV. The sources were collimated by a thick lead collimator, shown in Fig. 3, which was aimed at the center of the active LAr target.

Figure 5 shows the gamma-induced scintillation spectrum for 100000 events, after subtraction of a background spectrum scaled by the ratio of the lifetimes. This spectrum is similar to the ^{22}Na spectrum measured by the DarkSide-10 experiment [7], where the structure of the Compton scattering component and full energy deposition component of 511 keV and 1274 keV were shown in the spectrum in Fig. 5. Considering the thickness of the LAr target of the prototype was 8 cm, about $\frac{1}{3}$ the thickness of the DarkSide-10 detector, the ratio of full energy deposition component in the spectrum in Fig. 5 is much less than the ratio of the Compton scattering component. Therefore, the full energy components of 511 keV and 1274 keV are not obvious, and the most significant peaks in the spectrum of Fig. 5 are the Compton scattering components of 511 keV and 1274 keV gamma rays.

The Klein-Nishina formula describes the energy distribution of Compton scattered electrons [22]:

$$\frac{\mathrm{d}\sigma}{\mathrm{d}T} = \frac{\pi r_\mathrm{e}^2}{m_\mathrm{e} c^2 \alpha^2} \times \left(2 + \frac{s^2}{\alpha^2(1-s)^2} + \frac{s}{1-s}(s - \frac{2}{\alpha})\right) \tag{3}$$

where T indicates the kinematic energy of the scattered electron, $\alpha = h\nu/m_\mathrm{e}c^2$, and $s = T/h\nu$. Experimentally, the shape of the Compton scattering components detected by the detector could be described by the convolution of Eq. (3) and the Gaussian energy resolution. A Monte Carlo method could reproduce the spectrum by adding Gaussian smearing to Eq. (3). Figure 6 shows the spectrum of the convolution of Eq. (3) and various Gaussian energy resolutions.

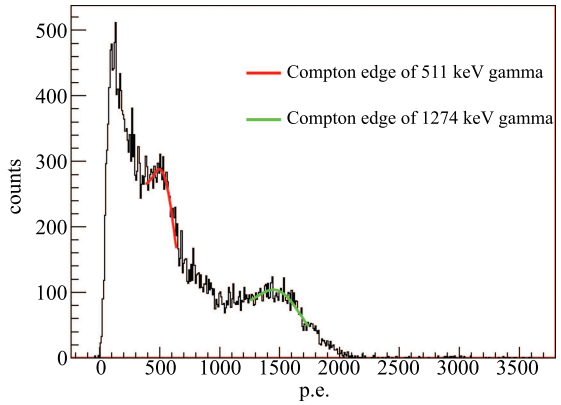

Fig. 5. (color online) The scintillation spectrum of ^{22}Na, after subtraction of a background spectrum scaled by the ratio of the lifetimes. Red: the Compton scattering of the 511 keV γ fitted with the convolution of Eq. (3) and a Gaussian energy resolution. Blue: the Compton scattering of the 1274 keV γ fitted with the convolution of Eq. (3) and a Gaussian energy resolution.

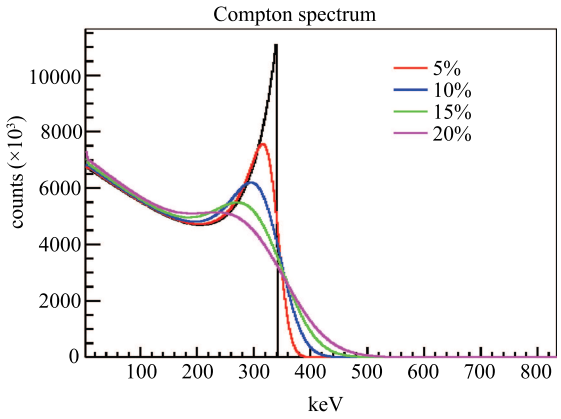

Fig. 6. (color online) The Compton scattering spectrum with various Gaussian energy resolutions. The energy of incident γ-rays was 511 keV. Black line: spectrum without energy spread, as shown in Eq. (3). Red line: spectrum with 5% energy resolution. Blue line: spectrum with 10% energy resolution. Green line: spectrum with 15% energy resolution. Pink line: spectrum with 20% energy resolution.

Figure 5 shows the two peaks fit with the convolution of Eq. (3) and the Gaussian energy resolution. The fit result shows that the light yield obtained from 511 keV γ was 1.64 p.e./keV, and the light yield obtained from 1274 keV γ was 1.53 p.e./keV.

To verify the two peaks shown in Fig. 5 were the Compton scattering spectrum, another measurement was carried out. The ^{22}Na source emitted two 511 keV gamma rays in opposite directions. The two back-to-back gamma rays could be used as a coincidence to generate a trigger to suppress noise and to get a clearer energy spectrum. The 70 μCi ^{22}Na gamma source was collimated by a thick lead collimator aimed at the center of the active LAr target. On the other side of the ^{22}Na source, another collimator was aimed at a plastic scintillator, which was used as the coincidence detector. The plastic scintillator used a 2" PMT as the photo detector.

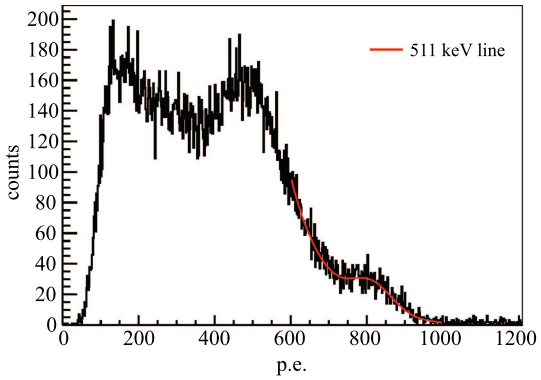

Fig. 7. (color online) Scintillation spectrum of ^{22}Na, triggered by back-to-back 511 keV gamma rays. Red: the 511 keV full-energy peak fitted with a Gaussian plus a falling exponential function.

Figure 7 shows the gamma-induced scintillation spectrum of 50000 events. Without the superposition of the 1274 keV γ spectrum, it shows a clear structure of Compton scatting component and full energy deposition component of 511 keV gamma rays, although the most significant peak is still the Compton scattering component. The full energy peak was fit with a Gaussian plus an exponential.

Table 1. The light yield obtained from Compton scattering of 511 keV and 1274 keV gamma rays together with the 511 keV full energy deposition peak.

E_γ/keV	fit method	LY/(p.e./keV)
511	Gaussian+Exp	1.59±0.02
511	Compton	1.64±0.02
1274	Compton	1.53±0.02

Comparing the two measurements, the following points could verify the view that the two peaks in Fig. 5 are Compton scattering components :

1) the spectrum in Fig. 7 shows a clear structure of Compton scattering component and full energy deposition component of 511 keV gamma rays. According to the relevant charge position, comparing the spectra in Fig. 5 and Fig. 7, it can be verified that the significant peak at about 500 p.e. is the Compton spectrum component of 511 keV gamma rays.

2) the light yield fitted by the Compton scattering spectrum in Fig. 5 agrees with the light yield from the

full energy peak fitted by the Gaussian plus a exponential in Fig. 7.

Several other liquid argon experiments, for example the DEAP-1 experiment [8, 24] and DarkSide-10 experiment [7], have reported their measurements of the light yield. Table 2 shows the light yield results, together with relevant LAr detector parameters, such as the PMT coverage, the quantum efficiencies[7, 23] of the PMTs and whether an Enhanced Specular Reflector (ESR) was used as the reflector[25].

Table 2. Light yield and several detector parameters of DarkSide-10, DEAP-1 and this LAr prototype. LY indicates the light yield; coverage, the PMT coverage of the detector; QE, the quantum efficiency of the PMTs; and ESR, whether or not ESR was used as the reflector

detector	LY[p.e./keV]	coverage(%)	QE(%)	ESR
this paper	1.6	9.6	25	no
darkside-10	9.1	19	34	yes
DEAP-1	2.7	20	28	no

According to Table 2, considering the low PMT coverage, low quantum efficiencies of the PMTs and lack of ESR reflector, the light yield obtained in this paper was relatively at the same level as the DEAP-1 and DarkSide-10 experiments.

6 Conclusion

Using the LN cooling system,and the domestically made argon purification system, a LAr prototype detector was set up. The LN cooling system combined with the commercial PID controller allowed the temperature fluctuation of the liquid argon to be controlled within less than 0.1 K during a one month run.

With a collimated ^{22}Na source, a proper energy spectrum showed about 1.59 p.e./keV light yield for 511 keV gamma rays. The light yield of the LAr prototype showed that the domestically made argon purification system worked well.

There is a positive correlation between light yield and PSD [15]. Therefore, it is crucial to achieve a higher light yield of the LAr detector to get better background suppression. In addition, larger light yield is helpful for the detector reaching the lower threshold [15]. To obtain higher light yield, the coverage of the PMTs will be increased and ESR will be used as the reflector to increase light collection in the future.

The result of the fit method by using the Compton scattering spectrum agreed with the result of the fit method using a Gaussian and a falling exponential. The fit method by using the Compton scattering spectrum was useful for the situation where the spectrum was degraded, leaving only the Compton edge as the most visible and reliable feature for light yield measurement.

References

1 P. A. R. Ade et al (Planck Collaboration), A&A, **571**: A16 (2014)
2 E. Aprile，T. Doke, Rev. Mod. Phys., **82**: 2053–2097 (2010)
3 D. Akerib et al (CDMS Collaboration), Phys Rev. Lett., **93**: 211301 (2004)
4 G. J. Alner et al (ZEPLIN Collaboration), Astropart. Phys., **28** :287 (2007)
5 P. Benetti et al (WArP Collaboration), Astropart. Phys., **28**: 495 (2008)
6 V. Sanglard et al (EDELWEISS Collaboration), Phys. Rev. D, **71**: 122002 (2005)
7 T. Alexander et al (DarkSide Collaboration), Astroparticle Physics, **49**: 44–51 (2015)
8 J. Walding et al (DEAP Collaboration), The DEAP-3600 Dark Matter Experiment, IOP 2013 - HEPP & APP Group Meeting (2015)
9 Q. Chen et al (CDEX Collaboration), arXiv:1512. 04258
10 K. Arisaka,P. Beltrame, C. W. Lam et al, Astroparticle Physics, **36**: 93–122 (2012)
11 M. Miyajima, T. Takahashi, S. Konno et al, Phys. Rev. A, **9**: 1438 (1974)
12 Akira Hitachi, Tan Takahashi, Nobutaka Funayama et al, Physical Review B, **27**: 5279 (1983)
13 M. Boulay, A. Hime, Astroparticle Physics, **25**: 179–182 (2006)
14 M. Boulay, Journal of Physics: Conference Series, **375**: 012027 (2012)
15 W. H. Lippincott, K. J. Coakley, D. Gastler et al, Physical Review C, **78**(3): 275–289 (2008)
16 Mark S. Cooke, Aip Conference Proceedings, **1182**(1-3):184-187 (2009)
17 B.Baptistaet, L. Bugel, C. Chiu et al, arXiv:1210.3793
18 Hamamatsu Photonics, R11065 data sheets (2009)
19 R. Acciarri et al (WArP Collaboration), Nucl. Instrum. Methods. A, **607**: 169–172 (2009)
20 http://www.teledynelecroy.com.cn/Upload/File/20150327162-324.pdf, retrieved 21st June (2013)
21 Shaoli Li et al (PandaX Collaboration), arXiv:1511.06223
22 N. Kudomi, Nuclear Instruments & Methods in Physics Research, **430**(1): 96–99 (1999)
23 ET Enterprises, 9390B series data sheets (2012)
24 P.-A. Amaudruzs et al (DEAP Collaboration), Astroparticle Physics, **62**: 178–194 (2015)
25 L. Baudis, G. Benato, R. Dressler et al, arXiv:1503.05349